






# Advanced Trajectory Planning and 3D Waypoints Navigation of Unmanned Underwater Vehicles Based Fuzzy Logic Control with LOS Guidance Technique

Fethi Demim<sup>1</sup><sup>a</sup>, Hadjira Belaidi<sup>2</sup><sup>b</sup>, Abdenebi Rouigueb<sup>3</sup><sup>c</sup>, Ali Zakaria Messaoui<sup>4</sup>,  
Kahina Louadj<sup>5</sup><sup>d</sup>, Sofian Saghour<sup>4</sup>, Mohamed Akram Benatia<sup>3</sup>, Mohamed Chergui<sup>6</sup>,  
Abdelkrim Nemra<sup>1</sup><sup>e</sup>, Ahmed Allam<sup>6</sup> and Elhaouari Kobzili<sup>6</sup>

<sup>1</sup>Laboratory of Guidance and Navigation, Ecole Militaire Polytechnique, Bordj El Bahri, Algiers, Algeria

<sup>2</sup>Signals and Systems Laboratory, Institute of Electrical and Electronic Engineering,  
University M'Hamed Bougara of Boumerdes, Boumerdes, Algeria

<sup>3</sup>Laboratory of Artificial Intelligence and Virtual Reality, Ecole Militaire Polytechnique, Bordj El Bahri, Algiers, Algeria

<sup>4</sup>Laboratory of Complex Systems Control and Simulators, Ecole Militaire Polytechnique, Algiers, Algeria

<sup>5</sup>Laboratoire d'Informatique, Mathématiques, et Physique pour l'Agriculture et les Forêts, Université de Bouira, Algeria

<sup>6</sup>Ecole Nationale Polytechnique, Algiers, Algeria

**Keywords:** Unmanned Underwater Vehicles, RRT, LOS Based Navigation Guidance, Fuzzy Logic Control, Avoiding Obstacle.


**Abstract:** Trajectory planning is a critical action for achieving the objectives of Unmanned Underwater Vehicles (UUVs). To navigate through complex environments, this study investigates motion trajectory planning using Rapidly-exploring Random Trees (RRT) and Fuzzy Logic Control (FLC). Our goal is to explore the use of the RRT trajectory planning algorithm to generate waypoints in a known static environment. In this case, the UUV's planned trajectory can meet the required conditions for obstacle avoidance. By using various objective functions, the model can be solved, and the corresponding control variables can be adjusted to effectively accomplish the requirements of underwater navigation. This technique has been successfully applied in various experimental scenarios, demonstrating the effectiveness of the FLC regulator. For instance, The 3D waypoint navigation challenge has been tackled by implementing the Fuzzy Controller, which utilizes the robust Line-Of-Sight (LOS) guidance technique. Experimental results demonstrate that the FLC regulator efficiently navigates through the waypoints, maintains an accurate course, controls the pitch and yaw angles of the UUV, and successfully reaches the final destination.


## 1 INTRODUCTION


Navigating Unmanned Underwater Vehicles (UUVs) in dynamic and uncertain underwater environments remains a formidable challenge. To tackle this, researchers are delving into advanced UUV navigation techniques like trajectory planning and control. Tra-


jectory planning, a critical facet of UUV navigation, involves charting a viable path from the current UUV position to the intended destination. This path must account for obstacle avoidance, seabed distance maintenance (Issac et al., 1979), disturbance compensation (e.g., ocean currents), and the preservation of desired stability levels (Breivik and Fossen, 2000).


To navigate around obstacles, UUVs often require additional power to come to a stop and remain stationary. In efforts to mitigate this challenge and enhance precision and effectiveness, research has ventured into employing Fuzzy Logic Controllers (FLCs) and artificial intelligence techniques (Blidberg, 2003)

<sup>a</sup>  <https://orcid.org/0000-0003-0687-0800>

<sup>b</sup>  <https://orcid.org/0000-0003-2424-626X>

<sup>c</sup>  <https://orcid.org/0000-0001-5699-2721>

<sup>d</sup>  <https://orcid.org/0000-0002-4203-6357>

<sup>e</sup>  <https://orcid.org/0000-0001-9237-9449>

(Coleman, 2003). Nonetheless, steering underwater vehicles remains intricate due to intricate interconnections, substantial nonlinearities in modeling, uncertainty in model parameters, and the complexities of handling disturbances like ocean currents and wave influences (Blidberg, 2003).

Over the past decade, a multitude of control techniques have emerged and undergone testing for autonomous underwater vehicles (AUVs). In 2018, diverse methods were introduced, including Optimization-technique based Adaptive Model-Free Control (OAMFC), adaptive backstepping terminal sliding mode control employing Recurrent Neural Networks (RNN), and an intelligent controller for cooperative missions with limited or no communication (Safaei and Mahyuddin, 2018) (Yang et al., 2018).

In 2022, two studies successfully addressed the challenge of fixed-time trajectory tracking control for underactuated AUVs in the presence of external disturbances. This achievement was attained by integrating the backstepping control technique with a fixed-time control approach (Peng et al., 2022) and (An et al., 2022). Looking ahead to 2023, an innovative trajectory planning method for AUV obstacle avoidance in complex environments emerged. This approach leveraged the Gauss Pseudo-spectral Method (GPM) and deep reinforcement learning to formulate a versatile trajectory planning model that accommodates multiple constraints (Gan et al., 2023).

This article introduces an advanced 3D trajectory planning and fuzzy logic control method for UUVs. The approach encompasses path generation with direct methods like the pseudo-spectral method (Kim and Kim, 2017), spanning theoretical foundations, practical implementation, and performance assessment. The article addresses fuzzy logic controller parameter optimization using techniques like Simulated Annealing, Genetic Algorithm, and Particle Swarm Optimization (Poppinga et al., 2011). To overcome current trajectory planning limitations, an enhanced mathematical model with dynamic constraints is proposed for precise navigation in complex underwater environments. The study employs an RRT-based algorithm and FLC controller for UUV trajectory planning and control, yielding enhanced navigation efficiency and empirical validation. Furthermore, it explores Fuzzy Controller integration for "Waypoints navigation" using RRT-generated way-points with LOS guidance, leveraging Simultaneous Localization and Mapping for advanced trajectory planning techniques (Demim et al., 2018), (Demim and et al., 2019), and (Demim et al., 2022).

The structure of the article is outlined as follows. Section II delves into UUV modeling, encompassing

both kinematic and dynamic equations. In Section III, a comprehensive exploration of the fuzzy logic control-based RRT algorithm is presented as a pivotal approach for UUV obstacle avoidance during 3D waypoint navigation. Moving on to Section IV, empirical findings are shared to validate the efficacy of the proposed methodologies. Finally, Section V concludes the paper by suggesting areas for future research work.

## 2 MATHEMATICAL REPRESENTATION OF UUV SYSTEM

### 2.1 Kinematic Modeling of UUV System

This section introduces a UUV trajectory planning method considering its physical capabilities and constraints. The dynamic model is described by six nonlinear equations for kinematics and dynamics, incorporating hydrodynamic and hydrostatic relationships governing 3D movement and stability. Euler angles  $(\phi, \theta, \psi)$  in a local coordinate system define the UUV's orientation, representing roll, pitch, and yaw rotations around the body-fixed frame's  $X$ ,  $Y$ , and  $Z$  axes (see Figure 1). Two coordinate systems are defined: the body-fixed frame and the earth-fixed frame, aligned with the UUV's center of gravity, forming the foundation for control and movement analysis. The

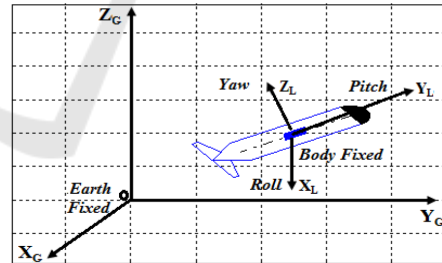


Figure 1: UUV presentation in the body-fixed frame.

UUV's center of gravity is defined in the absolute reference frame  $R_0$  by its Cartesian coordinates:

$$\eta_1 = [x, y, z]^T \quad (1)$$

The orientation of the vehicle, defined in the absolute reference frame, is expressed as:

$$\eta_2 = [\phi, \theta, \psi]^T \quad (2)$$

The position vector is expressed as:

$$\eta = [\eta_1^T, \eta_2^T]^T = [x, y, z, \phi, \theta, \psi]^T \quad (3)$$

The body-fixed velocity vector  $v$  of UUV is given by:

$$v = [v_1^T, v_2^T]^T = [u, v, w, p, q, r]^T \quad (4)$$

In this context, the vector  $v_1 = [u, v, w]^T$  denotes the linear velocities in surge ( $u$ ), sway ( $v$ ), and heave ( $w$ ) directions, corresponding to  $x$ ,  $y$ , and  $z$  axes. The vector  $v_2 = [p, q, r]^T$  signifies the angular velocities for roll, pitch, and yaw. The UUV's kinematic model allows trajectory determination based on initial configuration and translational and rotational velocities. The inertial reference frame linked to the earth yields the trajectory via the following kinematic relationship (Fossen, 2011):

$$\dot{\eta} = Jv \quad (5)$$

The Jacobian matrix  $J = T(\phi, \theta, \psi)$ , as derived from (Fossen, 1994), simplifies the translation of the UUV's position between global and local reference frames. This matrix enables the smooth conversion of coordinates between these frames, connecting them effectively. The relationship between global and local linear velocities  $[x; y; z]$  and  $[u; v; w]$  is encapsulated in the transformation equation:

$$\begin{bmatrix} u \\ v \\ w \end{bmatrix} = f(\phi, \theta, \psi) \times \begin{bmatrix} \dot{x} \\ \dot{y} \\ \dot{z} \end{bmatrix} \quad (6)$$

Modeling UUVs is a complex task and often involves challenges in determining hydrodynamic parameters, which can be addressed using empirical equations or tank tests. To simplify the modeling process, various assumptions can be made. First, we assume the UUV is neutrally buoyant and has a uniformly distributed mass. We also disregard roll motion, and external factors like wind, waves, and currents. Additionally, the dynamic equations incorporate a hydrodynamic drag term of less than two, while the UUV's structure is assumed symmetric across three main symmetry planes. The simplified kinematic equations (Eq. 5) (Liang et al., 2018) can be represented by neglecting roll motion ( $\phi = 0$ ):

$$\begin{cases} \dot{x} = u \cos(\psi) \cos(\theta) - v \sin(\psi) + w \cos(\psi) \sin(\theta) \\ \dot{y} = u \sin(\psi) \cos(\theta) + v \cos(\psi) + w \sin(\psi) \sin(\theta) \\ \dot{z} = -u \sin(\theta) + w \cos(\theta) \\ \dot{\theta} = q \\ \dot{\psi} = r / \cos(\theta) \end{cases} \quad (7)$$

## 2.2 Dynamic Modeling of UUV System

The equation of motion for an UUV depends on the effects of various control actions, such as rudder orientation, propulsion, gravity force, and buoyancy. As

UUVs are nonlinear systems, their dynamics can be modeled by the next equation (Yu et al., 2019):

$$M\dot{v} = C_{ext}(v)v + D(v)v + \tau_g + \tau_c \quad (8)$$

where  $M$  represents the positive definite symmetric inertia matrix,  $D(v)$  denotes the damping matrix, and  $C_{ext}(v)$  is the antisymmetric Coriolis and centrifugal forces matrix incorporating added mass effects. The vector  $\tau_{ext}$ , extracted from (Fossen, 2011), captures the forces and moments acting on the vehicle and can be deconstructed as follows:

$$\tau_{ext} = \tau_g + \tau_c \quad (9)$$

The vector  $\tau_{ext}$  of applied forces and moments can be partitioned into  $\tau_g$  and  $\tau_c$ . The former encompasses gravity and buoyancy-related forces and moments, while the latter originates from the vehicle's actuators. Hydrodynamic actuators can be categorized into rudders and depth control surfaces (corresponding to  $\tau_5$  and  $\tau_6$ , respectively), as well as propulsion force (represented by  $\tau_1$ ). Consequently, the vector of forces and moments resulting from the vehicle's actuators is given by:

$$\tau_c = [\tau_1, 0, 0, 0, \tau_5, \tau_6]^T \quad (10)$$

The UUV's dynamic model centers on the pivotal matrix  $M$ , encompassing mass and moments of inertia distribution. This matrix is pivotal for UUV motion modeling and force/moment calculations in response to water movements. Symmetrical UUV structure condenses  $M$  into a diagonal form, enhancing dynamics analysis across three principal symmetry planes.

$$M = \text{diag}[m_{11}, m_{22}, m_{33}, m_{44}, m_{55}, m_{66}] \quad (11)$$

Assuming that our vehicle is a rigid body with neutral buoyancy that satisfies  $W = B$  and has a homogeneous mass distribution, an even simpler representation can be obtained by locating the center of gravity and the center of buoyancy on the  $z$ -axis. This results in a simplified hydrostatic force representation as (Fossen, 2011):

$$\tau_g = \text{diag}[0, 0, 0, 0, -(z_G W - z_B B) \sin(\theta), 0] \quad (12)$$

The variables  $z_B$  and  $z_G$  represent the  $z$  position between the geometric center of the UUV and its center of buoyancy and center of gravity, respectively. We can rewrite equation 8 as follows:

$$\begin{cases} m_{11}\dot{u} = m_{22}vr - m_{33}wq - X_{uu}u - X_u|u|u| + \tau_1 \\ m_{22}\dot{v} = -m_{11}ur - Y_vv - Y_v|v|v| \\ m_{33}\dot{w} = m_{11}uq - Z_w w - Z_w|w|w| \\ m_{55}\dot{q} = (m_{33} - m_{11})uw - M_q|q|q| - (z_G w - z_B B) \sin(\theta) + \tau_5 \\ m_{66}\dot{r} = (m_{11} - m_{22})uv - N_r r - N_r|r|r| + \tau_6 \end{cases} \quad (13)$$

where  $\tau_1$  refers to the propulsion force,  $\tau_5$  and  $\tau_6$  express the pitch and yaw torques, respectively, and  $X_u, X_u|u|, Y_v, Y_v|v|, Z_w, Z_w|w|, N_r,$  and  $N_r|r|$  are the linear and quadratic drag terms coefficients (Fossen, 2011) (Liang et al., 2018).

### 3 FUZZY LOGIC CONTROLLER BASED UUV TRAJECTORY PLANNING

Waypoint navigation employing predetermined points for guiding UUVs through obstacle-rich environments is a widely utilized strategy. The Rapidly-Exploring Random Tree (RRT) algorithm excels at tackling intricate motion planning tasks, even within high-dimensional spaces. RRT's configuration tree construction and utilization of local planners make it particularly effective in dynamic and uncertain contexts. Moreover, the incorporation of advanced algorithms and optimization techniques enhances obstacle avoidance strategies and controllers, enabling the generation of real-time trajectories that adapt to external factors. In our study, we implemented the PD controller, a traditional option characterized by:

$$u(t) = K_p e(t) + K_d \frac{\dot{e}}{dt} \quad (14)$$

where  $e$  represents the error between the setpoint and the output,  $K_p$  and  $K_d$  represent the proportional and derivative gains, respectively. The fuzzy values are described as follows: *NVB* (Negative Very Big), *NB* (Negative Big), *NS* (Negative Small), *Z* (Zero), *PS* (Positive Small), *PB* (Positive Big), *PVB* (Positive Very Big),  $i \in \{1, 2, 3, 4, 5, 6, 7\}$ . The inference rules based on the Takagi-Sugeno technique are given in Table 1 which present the FLC Inference Rules for  $\tilde{\psi}$

Table 1: FLC Inference Rules.

$\tilde{\psi}/\tilde{\theta} \setminus \dot{\tilde{\psi}}/\dot{\tilde{\theta}}$	NB	NS	Zero	PS	PB
NB	NVB	NVB	NB	NS	PS
NS	NVB	NB	NS	PS	PS
Zero	NB	NS	Z	PS	PB
PS	NS	NS	PS	PB	PVB
PB	NS	PS	PB	PVB	PVB

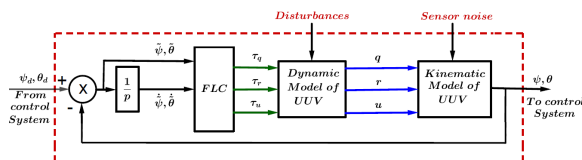


Figure 2: Fuzzy logic controller design.

and  $\tilde{\theta}$ , respectively. The problem of navigating UUVs through multiple passage points can be tackled by employing the RRT algorithm to generate a set of waypoints. This approach ensures a safe and viable trajectory in a known static environment. For controlling the UUV's pitch and yaw angles during 3D waypoint navigation, a Fuzzy Logic Controller (FLC) is implemented. The FLC governs the UUV's actions using the Line-Of-Sight (LOS) guidance method, enabling trajectory tracking while avoiding obstacles and maintaining stability. The integration of RRT and FLC streamlines waypoint navigation in challenging underwater conditions. The FLC control process, depicted in Figure 2, involves transforming input data using membership functions to linguistic terms and fuzzifying them to obtain degrees of membership. These are then used in a fuzzy inference system to generate an output control signal, which is subsequently defuzzified and converted into a specific value for UUV control. Notably, the calculation of  $\tau_q$  and  $\tau_r$  is as follows:

$$\tau_5 = \tau_q = FLC(e_\theta, \dot{e}_\theta) = \frac{\sum_{i=1}^m k_i \mu A(k_i)}{\sum_{i=1}^m \mu A(k_i)} \quad (15)$$

where  $\mu A(k_i)$  represents the degree of membership of the fuzzy variable  $\tau_q$  and  $k_i \in \{-200, -175, -100, 0, 100, 175, 200\}$  as shown in Figure 3(a).

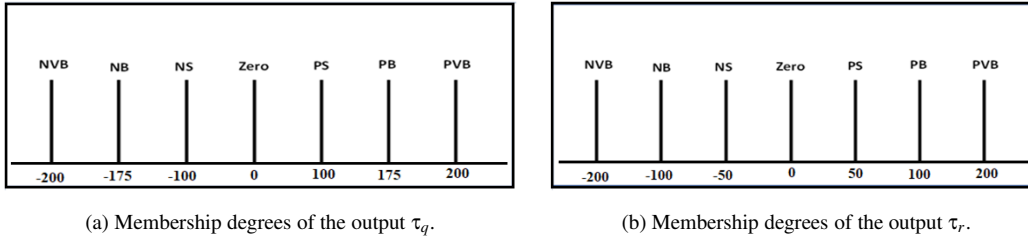
$$\tau_6 = \tau_r = FLC(e_\psi, \dot{e}_\psi) = \frac{\sum_{i=1}^m k_i \mu A(k_i)}{\sum_{i=1}^m \mu A(k_i)} \quad (16)$$

where  $\mu A(k_i)$  represents the degree of membership of the fuzzy variable  $\tau_r$  and  $k_i \in \{-200, -100, -50, 0, 50, 100, 200\}$  as shown in Figure 3(b).

### 4 LOS GUIDANCE PRINCIPLE FOR 3D TRAJECTORY PLANNING

The desired way-points  $p_d = (x_d, y_d, z_d)$  determine the input of the control structure. The desired heading and pitch angles are calculated based on the 3D LOS (Line-Of-Sight) guidance law. The FLC controller then assigns the desired torques to the vehicle to reach these way-points. The LOS strategy is based on aligning the vehicle as closely as possible to an imaginary straight line connecting the vehicle position and the target. Assuming it moves at a constant velocity  $u$ , the simple 2D-LOS for the desired heading angle  $\psi_d$  can be defined as follows:

$$\psi_{d_i} = \tan^{-1} \left( \frac{y_{d_i} - y}{x_{d_i} - x} \right) \quad (17)$$


 Figure 3: Presentation membership degrees of the output  $\tau_q$  and  $\tau_r$ .

The 3D guidance system is designed to adjust the desired depth of the UUV proportionally to its horizontal distance to the target. To achieve this, consider that the UUV needs to move from its current position  $(x, y, z)$  to the target waypoint  $(x_d, y_d, z_d)$ . The desired angle between the line connecting the UUV and the target and the horizontal plane, and can be calculated as follows:

$$\theta_d = \tan^{-1} \left( \frac{z_d - z}{\sqrt{(x_d - x)^2 + (y_d - y)^2}} \right) \quad (18)$$

where  $x_{d_i}, y_{d_i}, z_{d_i} : i = \{1, 2, 3, \dots, N\}$ ,  $N$  are the coordinates of the  $N$  waypoints in the plane  $XY$ , and  $(x, y, z)$  is the planar position of the UUV at time  $t$ .

## 5 EXPERIMENTS AND DISCUSSION

Our simulation results show that combining RRT with a fuzzy controller offers an effective and secure method for mission planning in realistic AUV operations. Fuzzy logic allows the creation of accurate models that closely resemble human reasoning. With its simplicity and versatility, fuzzy logic has remained a vibrant research area for several decades. Studies in fuzzy logic for process control have centered on establishing general design rules for fuzzy controllers, assessing stability criteria, and creating optimization algorithms for these controllers.

### 5.1 Tuning of the Controller Parameters

The simulation platform consists of an underactuated UUV model controlled by three independent inputs: propulsion force, pitch torque, and yaw torque. Its nominal values and hydrodynamic parameters are:

- **Inertia Terms:**  $\hat{m}_{11} = 215 \text{ Kg}$ ,  $\hat{m}_{22} = \hat{m}_{33} = 255 \text{ Kg}$ ,  $\hat{m}_{55} = \hat{m}_{66} = 80 \text{ Kg.m}^2$ ;
- **Linear Drag Hydrodynamic Coefficient Terms:**  $\hat{X}_u = 70 \text{ Kg/s}$ ,  $\hat{Y}_v = \hat{Z}_w = 100 \text{ Kg/s}$ ,  $\hat{M}_q = \hat{N}_r = 50 \text{ Kg.m}^2/\text{s}$ ;

- **Quadratic Drag Hydrodynamic Coefficient**

**Terms:**  $\hat{X}_u|u| = \hat{M}_q|q| = \hat{N}_r|r|100 \text{ Kg/m}$ ,  $\hat{Y}_v|v| = \hat{Y}_w|w| = 200 \text{ Kg/m}$ ;

- **Other Parameters:**  $m = 185 \text{ Kg}$ ,  $W = B = 1813 \text{ N}$ ,  $z_G = z_B = 0.01 \text{ m}$ ,  $\tilde{\psi} = \tilde{\theta} \in [-180^\circ, +180^\circ]$ ,  $\dot{\tilde{\psi}} = \dot{\tilde{\theta}} \in [-3, +3]$  and  $\tau_q, \tau_r \in [-200, +200]$ .

The control of the angles  $\psi$  and  $\theta$  is carried out by PD controller. These angles of the latter are written as follows:

$$\begin{cases} \tau_r = \tau_6 = K_p \tilde{\psi} + K_d \frac{\dot{\tilde{\psi}}}{dt} \\ \tau_q = \tau_5 = K_p \tilde{\theta} + K_d \frac{\dot{\tilde{\theta}}}{dt} \end{cases} \quad (19)$$

The error signals represent the differences between the desired and actual values of  $\psi$  and  $\theta$  as depicted in Figure 4. After incorporating the FLC controller with the calculated parameters into our system to regulate the angles  $\psi$  and  $\theta$ , we performed simulations and obtained the following results, as depicted in Figure 6:  $\psi_d = 0.57 \text{ rad}$ ,  $\theta_d = 0.52 \text{ rad}$ ,  $K_{p_r} = K_{p_q} = 7000$ ,  $K_{d_r} = 155.25$ ,  $K_{d_q} = 346$ . The FLC receives error signals, which represent the disparities between the desired and actual values of  $\psi$  and  $\theta$ , and employs fuzzy logic-based control rules to generate two control signals.

### 5.2 Comparison Between FLC and PD Controllers of Angles $\psi$ and $\theta$

We applied PD and FLC techniques for pitch and yaw angle control, with the objective of identifying an optimal controller that achieves steady-state error elimination, minimal overshoot, reduced settling time, and effective process regulation. Our aim is to devise a system characterized by precision, speed, stability, and robustness. To evaluate controller performance, the Mean Square Error (MSE) is commonly used as a parameter optimization metric, calculated as follows:

$$MSE_\psi = \frac{1}{N} \sum_1^N \tilde{\psi}^2, \quad MSE_\theta = \frac{1}{N} \sum_1^N \tilde{\theta}^2 \quad (20)$$

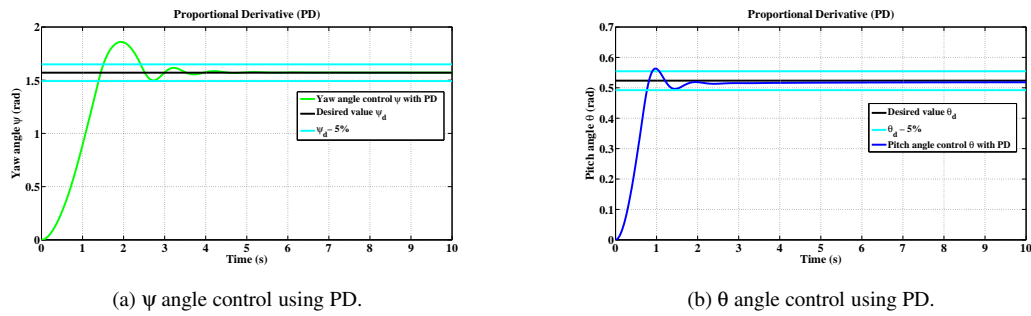


Figure 4: Control based PD of the angles  $\psi$  and  $\theta$ .

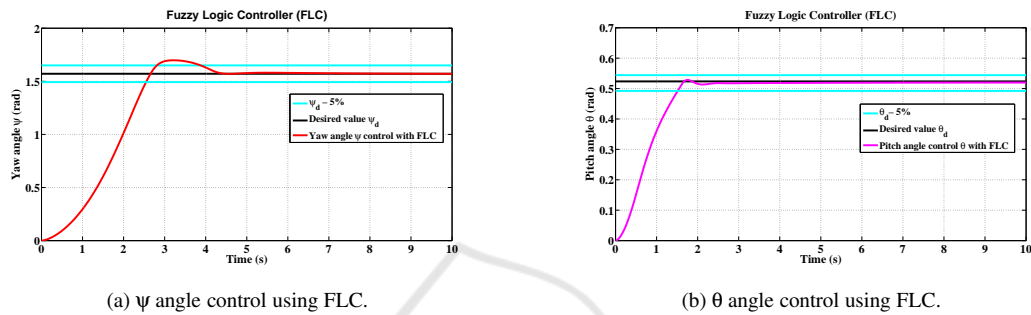


Figure 5: Control based FLC of the angles  $\psi$  and  $\theta$ .

where  $N$  represents the number of samples. In performance evaluation, accuracy is determined by comparing achieved goals to desired ones. This involves assessing the gap between desired setpoint and steady-state measurement, where  $\tilde{\psi}$  and  $\tilde{\theta}$  tend towards infinity. Speed is gauged by response time ( $T_{r\psi}, T_{r\theta}$ ), representing time to stable output within  $\pm 5\%$  of range. Damping links to damping ratio, indicating oscillation attenuation. Higher damping yields quicker damping, seen in overshoot ( $D_\psi, D_\theta$ ). Results in Table 2 show comparable, satisfactory performance of both controllers under steady-state. However, FLC surpasses PD, with reduced overshoot, enhanced precision, and lower mean squared error. PD has quicker response, but FLC boasts better damping, minimizing oscillations. FLC excels in precision, closely tracking trajectory with low MSE and aligned output. PD achieves speedier steady-state, yet larger overshoot could lead to oscillations (Table 2). Based on the findings in Table 2, the FLC controller proves advantageous for this system, exhibiting superior performance in terms of overshoot, precision, and MSE. However, if prioritizing speed over minimizing overshoot is crucial, the PD controller could be favored. Notably, our simulations reveal the FLC's overall superiority over the PD controller, except for response time. Figure 6 showcases a comparative analysis of the FLC-based and PD controllers' performance for  $\psi$  and  $\theta$ , affirming the FLC's superior tracking accuracy and overall performance. Furthermore, Figures 7 and

8 demonstrate the FLC-based control's effectiveness in regulating rotation velocities ( $q$  and  $r$ ) and torques ( $\tau_q$  and  $\tau_r$ ). The former illustrates angular velocity  $q$  and torque  $\tau_q$  aligning with the desired angle  $\theta_d$ , while the latter depicts angular velocity  $r$  and torque  $\tau_r$  aligning with the desired angle  $\psi_d$ .

### 5.3 3D Navigation by Waypoint Using the FLC-Based LOS Guidance Method

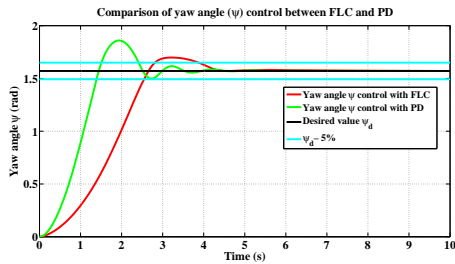
Figure 9 illustrates the UUV's 3D navigation along automatically generated waypoints from the RRT\* algorithm. The FLC-guided LOS controller ensures waypoint traversal while maintaining constant velocity. The control of  $\psi$  and  $\theta$  angles during navigation is displayed in Figures 10 and 11. The FLC employs input fuzzy sets for pitch and yaw angle errors and output fuzzy sets for pitch and yaw torques.

## 6 CONCLUSIONS

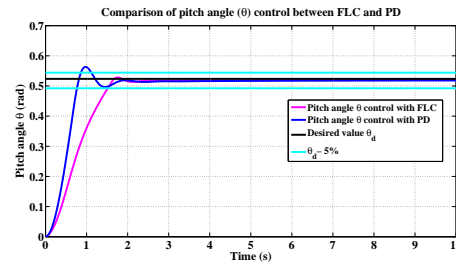
This article offers a comprehensive exploration of UUV trajectory planning, employing advanced RRT and fuzzy logic-based strategies. Our simulation results highlight the efficacy of combining RRT and fuzzy controllers for secure and efficient mission planning in challenging marine environments. Fuzzy

Table 2: Comparison of the angle  $\psi$  and  $\theta$  between FLC and PD Controllers.

Controller	$\psi$				$\theta$			
	$\frac{1}{N} \sum_1^N \tilde{\psi}^2$	$\lim_{t \rightarrow \infty} \tilde{\psi}$	$D_\psi$	$T_{r_\psi}$	$\frac{1}{N} \sum_1^N \tilde{\theta}^2$	$\lim_{t \rightarrow \infty} \tilde{\theta}$	$D_\theta$	$T_{r_\theta}$
FLC	9.2379e-11	-3.0409e-04	0.1271	3.88	1.4955e-08	-0.0039	0.0048	1.52
PD	1.1407e-10	3.3792e-04	0.2889	2.42	2.9002e-08	-0.0054	0.0397	1.12

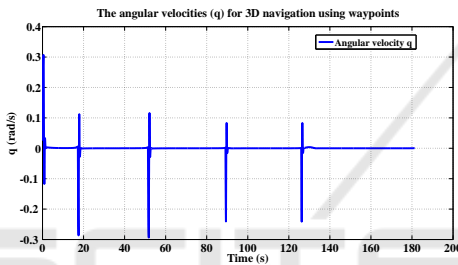


(a) Comparison of  $\psi$  angle control using FLC and PD.

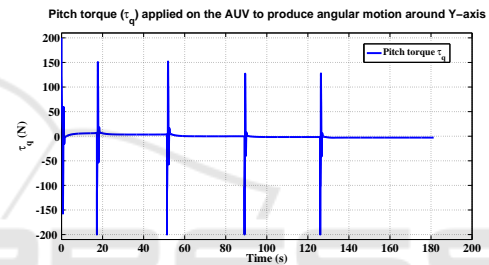


(b) Comparison of  $\theta$  angle control using FLC and PD.

Figure 6: Comparison control based FLC and PD of the angles  $\psi$  and  $\theta$ .

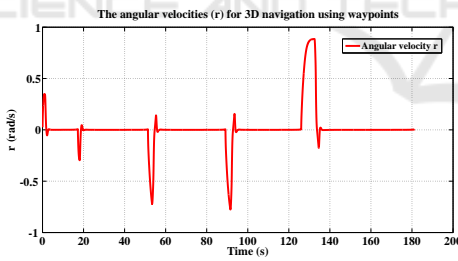


(a) Control of the rotation velocity  $q$ .

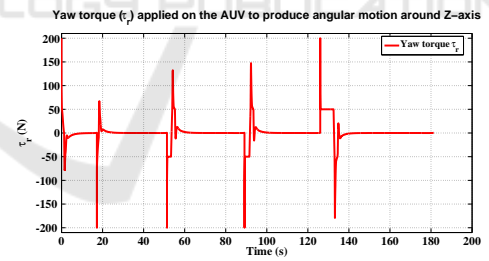


(b) Control of torque  $\tau_q$ .

Figure 7: Control of the rotation velocity  $q$  and torque  $\tau_q$ .



(a) Control of the rotation velocity  $r$ .



(b) Control of torque  $\tau_r$ .

Figure 8: Control of the rotation velocity  $r$  and torque  $\tau_r$ .

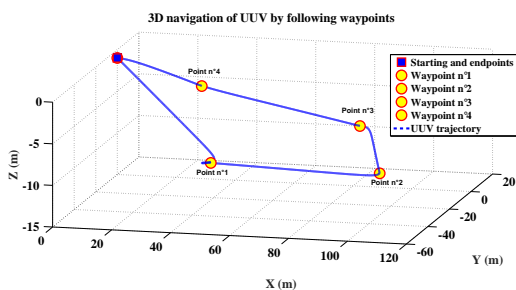


Figure 9: 3D navigation of the UUV by following waypoints.

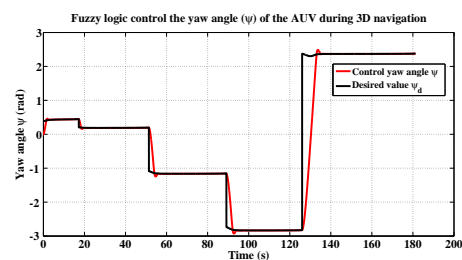


Figure 10: FLC controls the  $\psi$  angle during the 3D navigation trajectory.

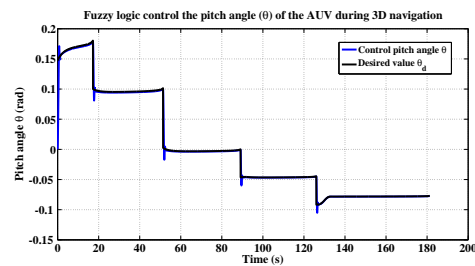


Figure 11: FLC controls the  $\theta$  angle during the 3D navigation trajectory.

logic mimics human-like representation and reasoning, making it a prolific research domain. Ongoing efforts in process control focus on developing general fuzzy controller rules, stability analysis, and optimization algorithms.

In our future research, we aim to incorporate integral square error analysis for a deeper understanding of FLC system performance compared to different controllers, emphasizing trajectory accuracy and stability. While our study holds potential, we recognize ongoing challenges in advancing UUV trajectory planning, requiring adaptable algorithms, seamless sensor integration, and addressing intricate mission scenarios. Tackling these challenges in upcoming research could greatly enhance trajectory planning efficiency, impacting diverse fields like oceanography, surveillance, exploration, and resource management.

## REFERENCES

An, S., Wang, L., and He, Y. (2022). Robust fixed-time tracking control for underactuated auvs based on fixed-time disturbance observer.

Blidberg, D. (2003). The development of autonomous underwater vehicles (auv). In *A Brief Summary, Autonomous Undersea Systems Institute, Lee New Hampshire, USA*.

Breivik, M. and Fossen, T. (2000). Guidance laws for autonomous underwater vehicles. In *Norwegian University of Science and Technology, Norway*.

Coleman, J. (2003). Undersea drones pull duty in iraq hunting mines. In *Cape Code Times*.

Demim, F., Benmansour, S., Nemra, A., Rouigueb, A., Hamerlain, M., and Bazoula, A. (2022). Simultaneous localization and mapping for autonomous underwater vehicle using a combined smooth variable structure filter and extended kalman filter. pages 621–650.

Demim, F. and et al., A. N. (2019). *NH- $\infty$ -SLAM algorithm for autonomous underwater vehicle*. Springer International Publishing.

Demim, F., Nemra, A., Abdelkadri, H., Louadj, K., Hamerlain, M., and Bazoula, A. (2018). Slam problem for autonomous underwater vehicle using svsf filter. In

*Proceeding of 25th IEEE International Conference on Systems, Signals and Image Processing, Maribor, Slovenia*, pages 1–5. IEEE.

Fossen, T. (1994). *Guidance and Control of Ocean Vehicles*.

Fossen, T. (2011). *Handbook of Marine Craft Hydrodynamics and Motion Control*.

Gan, W., Su, L., and Chu, Z. (2023). Trajectory planning of autonomous underwater vehicles based on gauss pseudospectral method.

Issac, M., Adams, S., He, M., Neil, W., Christopher, D., and Bachmayer, R. (1979). Manoeuvring experiments using the mun explorer auv. In *In proceeding*.

Kim, Y. and Kim, B. (2017). Time-optimal trajectory planning based on dynamics for differential-wheeled mobile robots with a geometric corridor. pages 5502–5512.

Liang, X., Qu, X., Hou, Y., and Ma, Q. (2018). Three-dimensional trajectory tracking control of an underactuated autonomous underwater vehicle based on ocean current observer. pages 1–9.

Peng, Y., Guo, L., and Meng, Q. (2022). Backstepping control strategy of an autonomous underwater vehicle based on probability gain. pages 39–58.

Poppinga, J., Birk, A., Pathak, K., and Vaskevicius, N. (2011). Fast 6-dof path planning for autonomous underwater vehicles (auv) based on 3d plane mapping.

Safaei, A. and Mahyuddin, M. (2018). Application of the optimal adaptive model-free control algorithm on an autonomous underwater vehicle. *Proceedings 3rd of the IEEE International Conference on Advanced Robotics and Mechatronics, Singapore, Singapore*.

Yang, C., Yao, F., and Zhang, M. (2018). Adaptive backstepping terminal sliding mode control method based on recurrent neural networks for autonomous underwater vehicle. pages 1–16.

Yu, H., Guo, C., and Yan, Z. (2019). Globally finite-time stable three-dimensional trajectory-tracking control of underactuated auvs.